J. Webster (ed.), *Wiley Encyclopedia of Electrical and Electronics Engineering*

TUNNELING AND JOSEPHSON JUNCTIONS

Tunneling devices incorporating superconducting materials can exhibit what are known as Josephson effects. A typical example is two superconducting materials separated by a thin dielectric barrier. Remarkably, such a tunneling device can exhibit both a zero-voltage trace for currents below some critical value and a second trace that has tunneling characteristics akin to a forward-biased diode. Traversing the entire current–voltage characteristic of the device will give a hysteretic current–voltage trace. The scale of these phenomena is roughly 1 mV for low-temperature superconductors (such as Pb, Pb-alloys, and Nb) and 10 mV for high-temperature superconductors (such as YBaCuO, BiSrCaCuO, and TlBaCaCuO).

Low-temperature superconductors used for Josephson applications have transition temperatures, T_c, from the normal to the superconducting state of approximately 1 K to 20 K, while high-temperature superconductors have $T_c \gtrsim 90$ K.

The zero-voltage leg of the current–voltage characteristics of a Josephson junction is highly sensitive to magnetic fields. This property is exploited by superconducting quantum interference devices (*SQUIDs*) to measure magnetic fields down to the 10 fT range, making them the most sensitive detectors of field/flux in existence. Superconducting quantum interference devices have been employed in prototype diagnostic systems for noninvasive mapping of heart and brain function, but must typically be operated within the confines of a magnetically shielded room. Prototype devices using *SQUIDs* for nondestructive evaluation of metal components are currently being tested in the field. *SQUIDs* are also employed in the detection of undersea anomalies (submarine and ordinance detection) and in a variety of scientific investigations such as earthquake, gravity-wave, free-quark, monopole, and dark-matter detection. Some practical *SQUID* devices have also used high-temperature superconductors.

The nonzero voltage leg of a Josephson junction current-voltage characteristic is also useful because it can be highly nonlinear. As such, these devices are employed for mixing in the 100 GHz region, where low noise-temperatures are a must (such as in radio astronomy). This work is restricted to low temperatures—on the order of 1 K—and the use of low-temperature superconductors. High-temperature-superconductor tunneling characteristics are not currently of sufficiently high quality for this application.

Another important potential application of Josephson junctions is their use in digital applications. The reason is that switching with Josephson-junction-based logic involves small voltages and currents and can occur over very short time scales. Intrinsic power and switching speed are in the 0.1 μW and 1 ps range. Josephson junctions employed for this purpose, based on Nb, are a mature technology. For a number of reasons, current technology has focused on ultrahigh-speed analog/digital conversion rather than computation; one issue is the current lack of a suitable memory format compatible with Josephson technology. Nevertheless, high-speed Josephson processing circuitry continues to have promise for such targeted applications as video image processing. A number of books and edited works are available on the subject of the Josephson effect and its applications (1,2,3,4,5,6,7,8).

Ironically, for digital and *SQUID* applications the intrinsic hysteresis of the junctions must be suppressed. For junctions that employ a thin, insulating oxide barrier, this implies the use of thin-film resistors to shunt the junctions to reduce the hysteresis. A better solution would be to tailor the tunnel barrier material so that

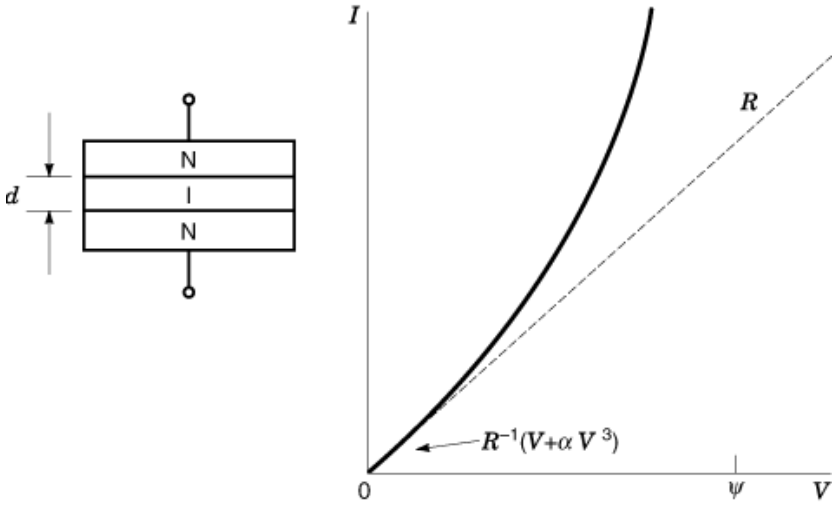

Fig. 1. Shown is a sketch of a normal–insulator–normal, *NIN*, tunneling system. N represents a normal, or nonsuperconducting metal film. I (nominally an insulator) represents a thin, dielectric layer through which quantum-mechanical tunneling can occur. The normal–metal films are typically approximately 10 nm to 100 nm thick and the dielectric layer is approximately 1 nm thick. Barrier heights, ψ are typically in the range of 0.1 eV to 3 eV. At low voltages $I \sim R^{-1}\,(V + \alpha V^3)$ with $\alpha \sim 1\ \mathrm{V}^{-2}$.

it was somewhere between a metal and insulator. More exactly, this suggests producing a material close to the metal-insulator transition. This subject is discussed at further length in connection with research in producing high-temperature superconductor junctions.

Metal–Insulator–Metal Tunneling

A basic tunneling system consists of a metal–insulator–metal (*MIM*) structure as depicted in Fig. 1. Generally the system comprises thin metal films ∼10 nm to 100 nm in thickness, separated by a thin dielectric layer $\gtrsim$1 nm in thickness. This dielectric can either be a native oxide created by the oxidation of the base metal electrode (a good example of which is aluminum) or a deposited artificial barrier, a good example of which is a semiconductor such as silicon. Tunneling in native and artificial barriers has been reviewed as a separate topic (9).

If the metals are not in the superconducting state, we have normal–insulator–normal (*NIN*) tunneling (10). The current–voltage characteristics of *NIN* junctions have been extensively studied in the context of quantum-mechanical electron tunneling through a potential barrier. The height of the barrier, ψ governs the rate of change of current with applied voltage. Barrier heights typically range from 0.1 eV to 3 eV. Simmons 11 has shown that for applied voltages $V \ll \psi$

$$I = R^{-1}(V + \alpha V^3)$$

where $\alpha \sim 1\ V^{-2}$.

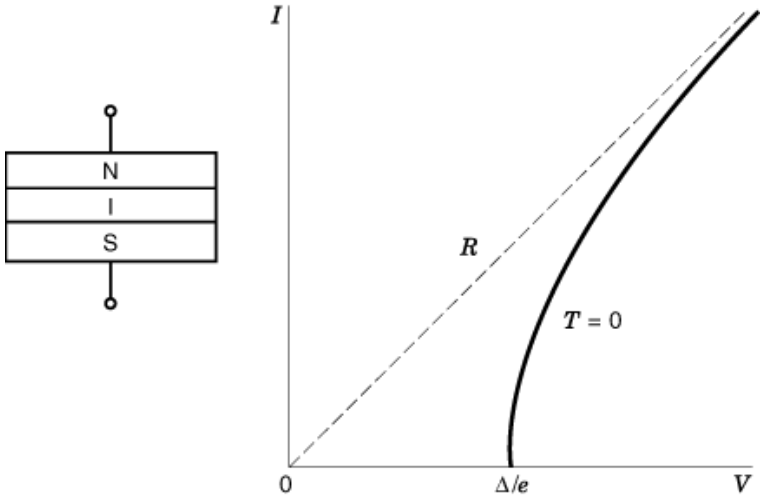

Fig. 2. Shown is a sketch of a superconductor–insulator–normal, *SIN*, tunneling system. N represents a normal, or nonsuperconducting metal film and S represents a superconducting film. I (nominally an insulator) represents a thin, dielectric layer through which quantum-mechanical tunneling can occur. The normal-metal films are typically approximately 10 nm to 100 nm thick and the dielectric layer is approximately 1 nm thick. The current–voltage trace shown is for zero temperature ($T = 0$).

At a given voltage, the current varies with barrier thickness, d and barrier height, ψas

$$I \propto \frac{\psi^{\frac{1}{2}}}{d} e^{-10.25\, d\psi^{\frac{1}{2}}}$$

where d is in nanometers and $\psi$is in volts (12). Tunneling in more complex although thematically similar semiconductor systems is discussed by Sze 13.

If we now introduce a superconductor (Fig. 2) as one of the metal elements of the tunnel junction, to produce a superconductor–insulator–normal (*SIN*) system, the current–voltage characteristic becomes highly modified. Most notable is the introduction of a region in which, at zero temperature, no current flows until a voltage Δ/e is reached, where Δ is the so called energy gap of the superconducting film. Energy gaps associated with conventional superconductors such as Pb, Pb alloys, Nb, NbTi, and NbSn are in the few meV (1 meV = 10^{-3} eV) range, while energy gaps associated with the high-temperature superconductor materials, such as YBaCuO, are in the $\gtrsim$30 meV range.

If we introduce a second superconductor to make an superconductor–insulator–superconductor (*SIS*) system, something unique occurs (Fig. 3). In this case, two branches develop in the system. If we start at zero current and increase the current slightly, no voltage will develop across the junction until the critical current, I_c, is reached. The critical current is related to the energy gaps of the superconductors by $I_c = \pi/4 \cdot (\Delta_1 + \Delta_2)/eR$, at zero temperature. For example, for Pb and Nb, $\Delta = 1.37$ and 1.53 meV, respectively.

If the critical current is exceeded, a junction driven by a current source will jump (at constant current) over to the quasi-particle curve. Further increasing the current moves one to higher voltages on the quasi-particle curve and reducing the current explores the rest of this curve. The zero-voltage state is not recovered until the current is reduced to zero. If a finite impedance source drives the junction, this switching will occur along the load-line of the system. This remarkable situation is due the fact that coherent tunneling of Cooper pairs of electrons (paired electrons in the superconducting state) can occur, producing a zero-voltage superconducting

tunneling state in the system. When the critical current is exceeded, these pairs are broken into quasi particles with properties akin to electron–hole pairs created across a semiconductor energy gap (13).

The current can be described by the Josephson equations (14,15,16)

$$I = I_c \sin \phi$$

where ϕ is the phase difference between the superconductors. Therefore, increasing the applied current from zero is equivalent to introducing a quantum-mechanical phase difference between the superconducting elements of the junction.

Beside *SIS* systems, properly configured SNS systems can also exhibit Josephson effects, as long as the normal-metal channel between the superconducting materials is of the appropriate geometry. This means that the normal metal is either a microscopic weak-link connection, point contact, or a thin-film metal constriction as opposed to a dielectric material (4,17).

Alternating Current Josephson Effect

A nonzero dc voltage, $V =$ constant, across a Josephson junction implies that

$$\frac{d\phi}{dt} = \frac{2e}{\hbar} V$$

which means that

$$\phi = \phi_0 + \frac{2e}{\hbar} Vt$$

Therefore, a finite voltage across a Josephson junction gives rise to a radio frequency (*RF*) current of

$$I = I_c \sin(\phi_0 + \frac{2e}{\hbar} Vt)$$

where $2e/h = 483.598$ THz V^{-1}. The presence of an alternating current associated with the appearance of a dc voltage across the junction is the ac Josephson effect. This means that at finite voltage, the current comprises a dc component with a superimposed ac modulation at the Josephson frequency. A current–voltage characteristic thus represents the time-averaged voltage across the junction as a function of applied current (when the system is driven by a finite-impedance source). The junction thus acts like an *RF* frequency-to-voltage converter.

Josephson junctions are in fact actually used as high-frequency sources. For a given junction, roughly 10 nW of power can be produced, although most this is dissipated in the junction resistance. The linewidth of the radiation is given by

$$f = \frac{2e}{h} V$$

where $\Phi_0 = h/2e = 2.068 \times 10^{-15}$ Wb is the magnetic flux quantum. For $T \sim 1$ K and $R \sim 1\ \Omega$, this means that $\Delta f \sim 1$ MHz. The linewidth can be reduced by coupling to a high-Q cavity, although with the concomitant loss of overall operational bandwidth.

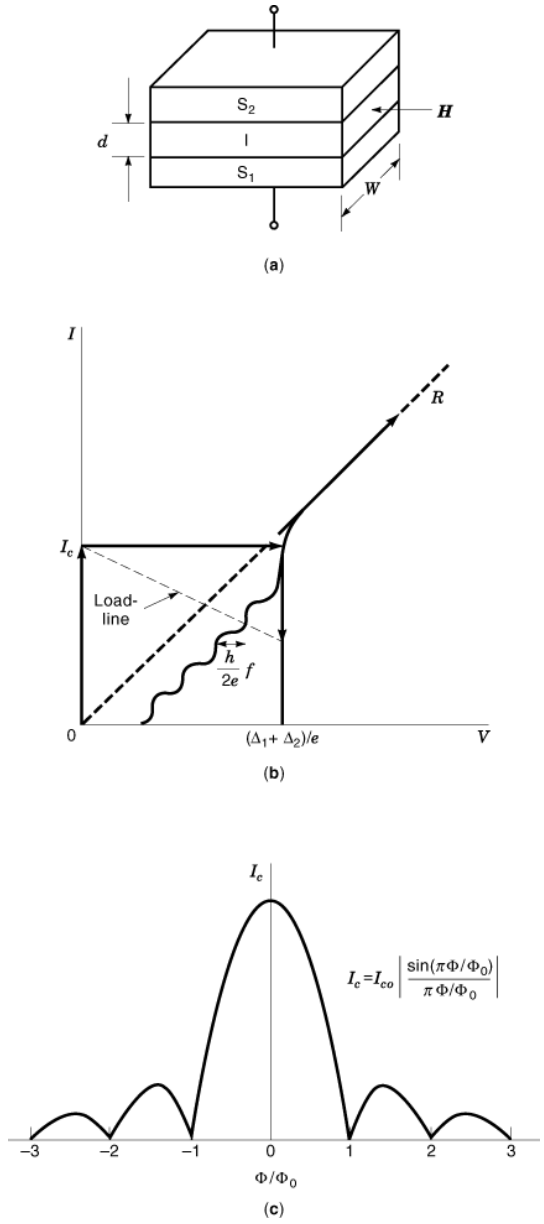

Fig. 3. Shown is a sketch of a superconductor–insulator–superconductor, *SIS*, tunneling system. S represents a superconducting film. I (nominally an insulator) represents a thin, dielectric layer through which quantum-mechanical tunneling can occur. The normal–metal films are typically approximately 10 nm to 100 nm thick and the dielectric layer is approximately 1 nm thick. Increasing the current applied across the device produces no voltage until the critical current, I_c is reached, at which point increasing or decreasing current drives the system along the nonzero-voltage, quasiparticle current–voltage characteristic. The load-line of a system driven by a nonzero impedance source is also indicated. Applying a magnetic field to a sufficiently small junction (see text) will produce a periodic depression of the critical current. Φ is the magnetic flux entering the junction. $\Phi = HW(d + \lambda_1 + \lambda_2)$, where λ is the penetration depth and $\Phi_0 = h/2e = 2.068 \times 10^{-15}$ Wb.

To achieve useful output power levels, arrays of junctions are produced to create tunable millimeter wave sources—typically as low-noise local oscillators for radio astronomy mixer applications. Junction arrays can produce ~2 μW to 6 μW of *RF* power in the 340 GHz to 440 GHz band. To achieve this, all junctions in the array must be phase locked (18).

The ac Josephson effect can be manifested as Shapiro steps (Fig. 3) by coupling microwave radiation into the junction. This produces a series of steps of equal width $\Delta V = (h/2e)$ where f is the frequency of the applied microwaves. An important application that exploits this phenomenon, and also uses series arrays of (here Nb-based) junctions, is the standard volt. Here, a junction array is driven by a microwave source to produce in excess of 1 V dc on the output terminals of the device (19,20). Only fundamental constants and the frequency of an external oscillator, which can be established with high accuracy, determine the output voltage. The National Institute of Standards and Technology (*NIST*) has developed Josephson arrays for this purpose and they now serve as the primary US standard volt.

Recent work in this particular area has also included Nb/AuPd/Nb (SNS-type) junctions. These systems use a normal–metal alloy instead of a dielectric barrier, through which Josephson coupling can also occur to produce a junction that is inherently resistively shunted (21). Another refinement is to use Ti (22) instead of AuPd. Titanium is potentially more desirable, because its resistivity (at 4.2 K) is higher than AuPd and it is compatible with whole-wafer processing techniques.

Experimental work based on a stacks of Josephson junctions (23) has also been explored for potential submillimeter oscillator applications with, for example, NbCN/MgO/NbCN (24), NbCN/NgO/NbCN (25), and Nb/Al/AlOx/Nb (26,27) systems. Stacks of Josephson junctions may also be useful as inductive elements in resistive or rapid single-flux-quantum (*RSFQ*) digital circuitry. One technical challenge here is producing junctions with uniform Josephson critical currents, I_c (28).

Microwave irradiation has also been explored on a more purely experimental basis with high-temperature superconductors. These materials can be viewed as a stack of superconducting CuO planes, with an interplanar quantum-mechanical coupling that can vary from one material to another. For example, the layer-to-layer coupling in BaSrCaCuO is far less than in YBaCuO. In fact, in the former case the coupling is similar to the Josephson coupling occurring in an *SIS* tunnel junction. Thus BaSrCaCuO is thought capable of mimicking the behavior of a stack of individual Josephson junctions. With this picture in mind, researchers have applied microwave radiation to BaSrCaCuO mesas. Microwave steps were in fact observed, but with a voltage spacing greater than that expected for Shapiro steps (29). Mesa-type TlBaCaCuO devices have also been produced (30) with microwave applications in mind. Again, however, these systems remain experimental in nature.

Magnetic-Field Effects

The current distribution in a Josephson junction will be uniform if the width, W, of the junction (see Fig. 3) is small compared with the Josephson penetration depth, λ_J, with

$$\Delta f = \frac{4k_B TR}{\Phi_0^2}$$

where $J_c = I_c/A$ with A the junction area, and $t = \lambda_1 + \lambda_2 + d$. The quantities λ are the penetration depths of the superconductors composing the junction. This is the scale over which an applied external magnetic field will penetrate into a superconductor. Here d again is the thickness of the barrier (1,2,3,4,5,6,31).

In the case where we apply a static magnetic field to the junction along the direction of the plane of the barrier, we will suppress the Josephson current. If we meet the criterion that the junction is small compared

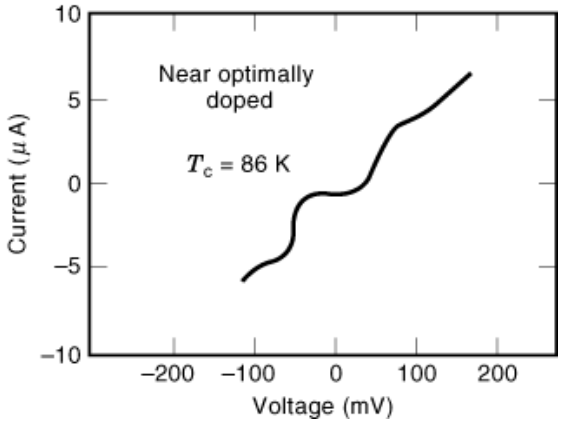

Fig. 4. Shown is the current–voltage characteristic of a nominally *SIS* junction created by using a scanning tunneling microscope tip to peel up a portion of the surface of a high-temperature superconducting BiSrCaCO (2212) film and hold it in proximity to the underlying material. Although not an ideal characteristic, this demonstrates the ability to achieve (and provides a means to study in detail) tunneling in the high-temperature superconductor materials. From Miyakawa et al., Ref. 32.

with the Josephson penetration depth, this suppression of the critical current will take the form

$$\lambda_J = \left\{ \frac{h}{2e\mu t J_c} \right\}$$

where I_{c0} is the zero-field critical current. For Pb, Nb, NbSn, $\lambda \sim 50$ nm to 100 nm; for NbN, $\lambda \sim 300$ nm; and for YBaCuO $\lambda_{\parallel} \sim 30$ nm and $\lambda_{\perp} \sim 200$ nm. In the last case, parallel and perpendicular refer to the directions along and perpendicular to the CuO planes.

If a junction is not small by this definition, the current distribution will not be uniform and the suppression of the critical current will not follow the simple sinx/x behavior noted above. Indeed, the geometry of the junction can be controlled to produce a critical-current behavior parametrically tailored to specific applications, as in the case with the use of junctions as elements for digital applications. In addition, the spatial nonuniformity of the barriers of individual junctions can be diagnosed through a deconvolution of critical current versus applied magnetic field characteristics (3).

As far as applications are concerned, this general phenomenology implies that a large penetration depth is generally undesirable. A material such as NbN, which has a larger energy gap than Nb (and from this standpoint represents a superior material) suffers from this limitation. However, this can be in part engineered around by creating hybrid NbN/Nb layer pairs in which a balance of the higher critical temperature of NbN (14 K as opposed to 9.25 K for Nb) and lower penetration depth of Nb is reached. Another important example of the use of hybrid materials systems also involves Nb as Nb/Al bilayers; these are used to produce high-quality tunnel junctions as is discussed later (see section entitled "Digital Applications.")

Finally we note that *SIS* junctions have been made with high-temperature superconductor materials as well. As shown in Fig. 4, such devices have been created with the use of a scanning tunneling microscope tip which is "crashed" into the surface of a BiSrCaCuO crystal (32). As the tip is pulled back up, a junction is created between superconducting material remaining on the tip and the underlying crystal. While hardly a practical device, with less-than-perfect current–voltage characteristics, this nonetheless illustrates the potential for creating devices from high-temperature superconductor material and has provided a valuable vehicle for fundamental studies of the system.

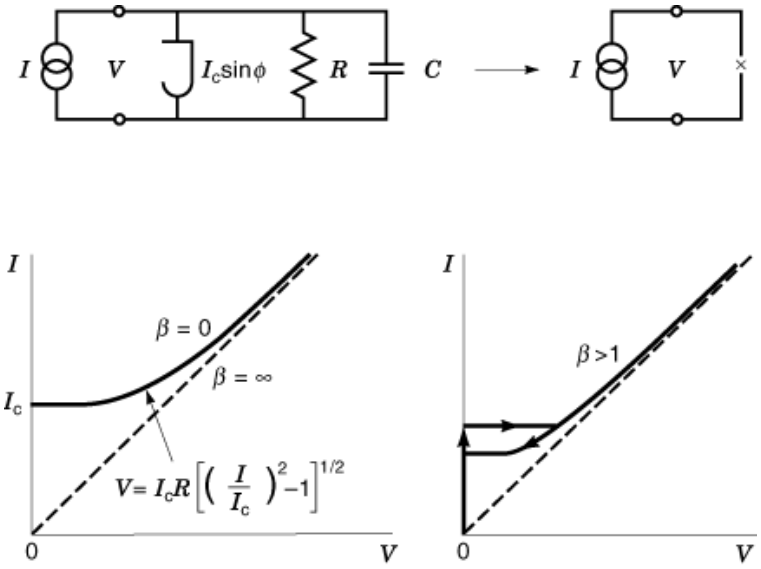

Fig. 5. The resistively shunted junction (*RSJ*) model for tunneling in *SIS* systems. This diagram illustrates that the degree of hysteresis in a junction with a given resistance and capacitance is governed by the magnitude of the parameter $\beta = (2e/h)I_c R^2 C$. The parameter can be viewed as setting the degree of damping in the circuit.

The Resistively Shunted Junction (*RSJ*) Model

The application of Josephson junctions generally requires control of the degree of junction hysteresis. One way of achieving this is to shunt the junction with an external resistor. This usually means the use of a thin film of Au or AuCu alloy deposited across the *SIS* junction to produce a shunt in the range of ~1 Ω. In some cases, junctions can be produced with internal microscopic resistive links in the barrier layer to achieve the same effect. More sophisticated approaches, involving tuning the properties of tunnel barriers to achieve a conductivity near the metal–insulator transition, have also been proposed and are discussed further in "High-Temperature Superconductor Ramp Junctions."

Figure 5 shows the electrical equivalent circuit of a shunted Josephson junction with a total resistance R biased by a current source (shunted with an external resistor to produce a resistance far lower than the original tunneling resistance of the junction). Represented in this manner there are three current paths: the Josephson current, the ohmic current, and the displacement current from the junction capacitance. The total current (for a system driven by a current source) is thus

$$\frac{I_c}{I_{c0}} = \left|\frac{\sin \pi(\Phi/\Phi_0)}{\pi(\Phi/\Phi_0)}\right|$$

Along with the Josephson relation

$$I = I_c \sin \phi + \frac{V}{R} + C\frac{dV}{dt}$$

this can be rewritten as

$$V = \frac{\hbar}{2e}\frac{d\phi}{dt}$$

where $\omega_c = (2e/)I_cR$ represents the upper operational frequency of the junction and $\omega_p = (2eI_c/C)^{1/2}$ is the "plasma" or lower-bound propagation frequency of the system. It is customary to define the Stewart–McCumber parameter

$$\frac{I}{I_c} = \sin\phi - \omega_c^{-1}\frac{d\phi}{dt} + \omega_p^{-2}\frac{d^2\phi}{dt^2}$$

The dependence of the current-voltage characteristics of a Josephson junction on β is also depicted in Fig. 5. Small and large values of β represent the high- and low-damping limits, respectively. The most desirable operating regime for many applications is $\beta \sim 1$. As noted by Likharev 4, a useful way of parameterizing β is as

$$\beta = \left(\frac{\omega_c}{\omega_p}\right)^2 = \frac{2e}{\hbar} I_c R^2 C$$

where again $J_c = I_c/A$, A is the junction area (W^2 in Fig. 3), ϵ_r is the dielectric constant of the junction barrier material, $\epsilon_0 = 8.85 \times 10^{-12}$ F/m, and d is the barrier thickness. Improved performance at high frequencies generally implies smaller areas and a concomitant increase in J_c to achieve $\beta \sim 1$ (33). Note that in principle

$$\beta = \frac{2e}{\hbar}(I_c R)^2 \frac{\varepsilon_r \varepsilon_0}{d} J_c^{-1}$$

is an intrinsic property of the superconductors. Its actual value, however, can be lower than the indicated theoretical result due to gap suppression at film surfaces and other effects.

Superconducting Quantum Interference Devices

If we place two Josephson junctions in a loop (Fig. 6) we form a *SQUID*, in this case a so-called dc *SQUID*. To produce a device intended for the measurement of flux, the junctions are shunted, as discussed previously, to suppress junction hysteresis. The flux associated with an applied magnetic field generates a circulating current in the device, which suppresses the Josephson current. An applied flux thus modulates the voltage across the device with a period equal to the magnetic flux quantum Φ_0. The result of this is a device that is very sensitive to magnetic flux. *SQUIDs* are sensitive to flux to magnitudes $\Phi_{\text{applied}} \ll \Phi_0 = h/2e = 2.068 \times 10^{-15}$ Wb. Practical *SQUIDs* are capable of measuring fields to the 10 fT magnetic field range, or $\sim 10^{-34}$ J·Hz^{-1} at 10^5 Hz (34,35), making them by far the most sensitive device in existence for measuring magnetic fields and flux. Field versions of *SQUIDs* can usually achieve an order of magnitude more sensitivity than flux gate magnetometers.

SQUIDs have a variety of applications, including commercial biomedical *SQUID* arrays that noninvasively monitor and map heart and brain function. Other uses include nondestructive evaluation (*NDE*) (e.g., crack detection in metals), oceanic anomaly detection, gravity-wave antennas, earthquake monitoring, magnetic monopole detection, dark-matter searches, and other fundamental scientific investigations (6,36,37).

A key factor limiting the performance of *SQUIDs* is $1/f$ noise. This stems from shallow trapping of both fluxoids in the thin-film elements of the *SQUID* and tunneling electrons in the barriers of the Josephson junctions (shot noise). The observed $1/f$ noise typically has a knee in the 1 Hz to 10 Hz range with an associated spectral flux noise density $\gtrsim 10^{-10}\ \Phi^2{}_0/\text{Hz}^{-1}$ at 0.1 Hz. Optimizing *SQUID* performance is especially important for biomedical applications since operation down to the 0.1 Hz range is necessary (38).

The flux noise energy of a *SQUID* can be written as (39)

$$I_c R = \frac{\pi}{4}\frac{\Delta_1 + \Delta_2}{e}$$

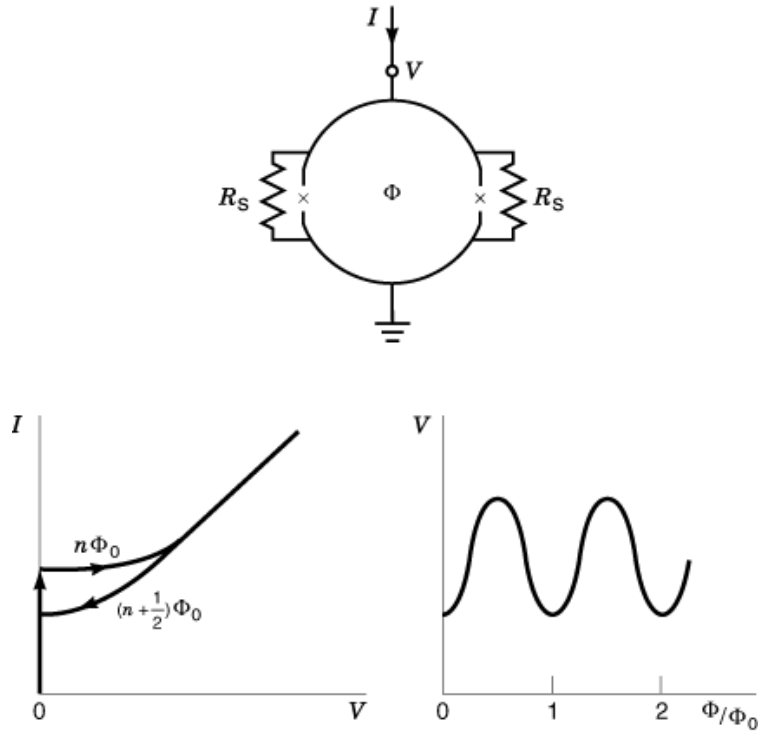

Fig. 6. Shown is a sketch of a dc *SQUID* (superconducting quantum interference device) comprising a loop with two Josephson junctions. Shunt resistances are used to control the damping parameter (β) of the junctions. The current–voltage characteristics and voltage–flux characteristics are shown for an applied flux Φ.

which generally suggests the need for devices with the smallest inductance and capacitance, operating at the lowest temperatures. The use of low-temperature superconductors (Pb, Pb-alloys, Nb, and so on) generally means operation at 4.2 K, (the boiling point of liquid helium at 1 atm) and temperatures less than 80 K for the high-temperature superconductor materials. A method successfully used to reduce inductance is the washer loop (39). Because of the Meissner effect associated with superconductivity, flux transformers can be used to collect and couple flux from a larger, external superconducting loop and present it to the *SQUID* using a multiturn thin-film coil.

High-temperature superconductors have also been relatively successfully explored for *SQUID* applications. An approach to creating Josephson junctions in high-temperature superconductor materials is to simply make a step in a substrate to create a step-edge junction. Material grown across the edge acquires a defect that creates a weakly linked Josephson junction, with characteristics similar to a resistively shunted *SIS* system. It was realized that the actual angle of the step or ramp was important in consistently creating junctions with desired characteristics (40,41,42). Along the same lines, junctions made with silicon-on-sapphire (*SOS*) substrates have demonstrated *RSJ* characteristics (43,44) and were used to make the first *SQUIDs* operating at 77 K using step-edge techniques (45).

A different approach to the use of high-temperature superconductor materials is the use of bicrystal substrates. Here, two single crystals (for example, of $SrTiO_3$) are fused together at a predetermined angle to create an off-axis interface. Junctions are made by depositing a thin film of high-temperature superconductor material across this disruptive interface. Bicrystal work in particular has consistently shown *RSJ*-type current–voltage characteristics and critical currents that are reproducibly correlated to the angular displacement of the

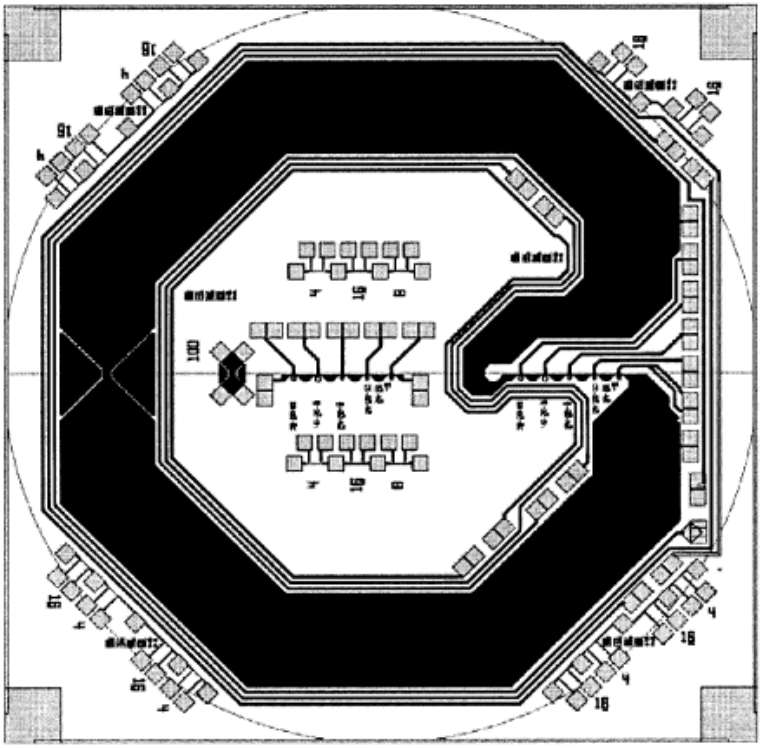

Fig. 7. *SQUID* structure from IBM. Most of the structure seen in the figure is the superconducting loop containing a "flux dam," visible as the triangular restriction on the left, to reduce device noise by limiting circulating currents in the flux loop lines. The Josephson junctions incorporated into the structure are step-edge devices. The overall size of the *SQUID* is 1 × 1 cm. From Sun et al., Ref. 53.

substrate crystal lattices. These bicrystal junctions have been successfully incorporated into YBaCuO (46,47,48) and BaSrCaCuO *SQUIDs* (49,50). Bicrystal junctions of MgO (51) have also been discussed for use in *SQUIDs* targeted for nondestructive evaluation systems. Noise studies (52) suggest that bicrystal and step-edge techniques generally produce devices of comparable quality. However, although the techniques are suitable for few-device applications such as *SQUIDs*, they are not appropriate for medium- or large-scale integration.

The practical implementation of high-temperature *SQUID* technology is shown in Fig. 7. The work is from Koch's group at IBM (53). Here junctions are formatted into a large loop containing *flux dams*, one of which is shown to the left as a constriction in the loop. The constriction creates a fuselike link to help eliminate noise-generating current loops.

Beside the double-junction dc *SQUID*, there is also the single-junction *RF SQUID*, depicted in Fig. 8. With this device, flux quantization in the ring, along with the corresponding variation of the Josephson current with flux, produce a variation in the inductance of the *SQUID* loop. This change in loop inductance is coupled to and thus shifts the resonant frequency of an external, *RF*-driven tank circuit. Because of its relative simplicity and the requirement for only a single, shunted Josephson junction, this scheme was initially and has continued to be the device of choice for many commercial applications, notably for nondestructive evaluation and *SQUID* voltmeters.

We note finally that, irrespective of the type of *SQUID* employed, applications such as biomedical diagnostics typically require operation within the confines of a carefully shielded magnetic enclosure. However, for

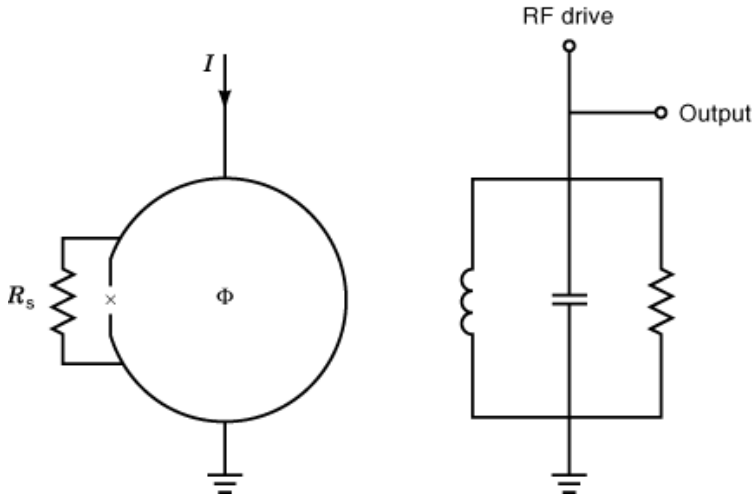

Fig. 8. Shown the schematic of an *RF SQUID*. This type of *SQUID* uses a single (shunted) Josephson junction in a loop. Applied external flux (Φ) acts to alter the impedance of the loop, which is inductively coupled to and shifts the frequency of an *RF* driven tank circuit.

such applications such as nondestructive evaluation field work, *SQUID* gradiometers can be employed that are more immune from background magnetic fields and can be optimized for unshielded performance. This implies a compromise between field sensitivity and voltage modulation characteristics. For example, *SQUIDs* for nondestructive evaluation (54) are cited as having a flux noise at 1 Hz of 134 $\mu\Phi_0\text{Hz}^{-1/2}$ and 60 $\mu\Phi_0\text{Hz}^{-1/2}$ at 10 Hz, qualifying them as prototype commercial systems (55).

In addition to the measurement of flux, *SQUIDs* can also be configured to perform other functions. This includes the measurement of ultrasmall voltages. *SQUID* voltmeters are commercially available for measurements in the 1 pV range—limited by noise to a range of $\sim 10^{-10}$ V/Hz$^{-1/2}$ at 100 Ω. Radio frequency *SQUIDs* have also been employed as low-noise amplifiers to ∼100 MHz.

Mixing and Detection

The zero-voltage branch of a Josephson junction (Fig. 3) can respond at frequencies up to $f \sim (4\Delta/h) \sim (e/h)I_cR \gtrsim 1$ THz for low-temperature superconductors and $\gtrsim$10 THz for high-temperature materials. As a result high-frequency Josephson mixing has been extensively studied. Unfortunately, heterodyne mixing using the zero-voltage branch of the Josephson tunneling characteristic is seriously degraded by the appearance of excess noise due to noise down conversion and the dynamic impedance related to the ac Josephson effect (56).

However, the extreme nonlinearity of the quasi-particle portion of the current–voltage characteristic, as the tunneling current turns on for voltages just above the sum-gap voltage, has been successfully exploited for mixing (56,57,58) in the same manner as high-frequency diodes are used. For superconducting mixing, the Josephson current (zero-voltage curve) becomes a nuisance and can be suppressed by applying a small magnetic field. Such devices are generally referred to as *SIS* mixers, with maximum operating frequencies the same as noted previously.

SIS mixers are typically employed when uncompromising low-noise performance is required (such as with radio astronomy) and where very low (∼1 μW) local-oscillator power is required. These mixers are typically used in the ∼40 GHz to 1 THz region, with single sideband (*SSB*) noise temperatures at 100 GHz of ∼4 K. Overall

noise temperatures for ∼40 GHz to 1 THz are typically within an order of magnitude of the quantum noise limit of hf/k_B. This currently exceeds the performance of high-electron-mobility transistor (*HEMT*) devices.

One critical element in mixing is junction quality. The magnitude of the tunneling current for voltages below the turn-on voltage for quasi-particle tunneling, that is, voltages below the sum-gap voltage, is a crital factor in mixer noise performance. Leakage conduction in this regime needs to be as small as possible and is limited in theory only by thermal excitations, but in practice can be dominated by imperfections in the tunnel barrier itself. For this reason, junctions based on oxidized tin and other soft metals were initially employed because of their extremely low so-called subgap conductance due to the high quality of the Sn-oxide barrier. However metals such as Sn are not physically robust with respect to thermal cycling (from their ∼1 K operating temperature to room temperature).

Mixing requires a very high quality dielectric barrier integrated into superconductive elements with the highest possible energy gap (and hence critical temperature) to provide the highest operating frequency. Matching requirements also mean that junction resistance be in the 20 Ω to 100 Ω range and that $1 < 2\pi RCf < 10$. Practical compromises have resulted in the use of hybrid systems such as Nb-based electrodes, aluminum-oxide barriers, and Pb-alloy counterelectrodes to form Nb–Al_2O_3–Pb-alloy junctions. This is a good union between the thermal stability of Nb and the high-quality dielectric properties of Al_2O_3. Nb–Al_2O_3–Nb junctions have also been adopted for mixing applications. The upper operational limit for Nb-based junctions is ∼1.3 THz. Junctions based on NbN (with a critical temperature of ∼14 K compared with the 9.25 K transition temperature of niobium) have also been made, which have an operational mixing limit of ∼2.5 THz. Early NbN work explored both NbN–MgO–NbN (59,60), and NbN–AlN–NbN systems (61,62,63). Recent NbN work has produced devices with double sideband receiver noise temperatures of 1450 K at 600 GHz and 2800 K at 950 GHz (64).

Mixing experiments have also been conducted with high-temperature superconductor materials. For example, bicrystal silicon-based junctions have been produced for this purpose (65). Bicrystal results on silicon and sapphire (66) appear to be comparable to those achieved with $SrTiO_3$ in terms of the overall nature of their current–voltage characteristics, but without the disadvantage of the large dielectric effects of $SrTiO_3$. Both Shapiro steps (67) and harmonic mixing of a 1.6 THz signal have been observed (68) in such systems. However, high-temperature superconductor tunnel systems that have demonstrably fulfilled the stringent requirements for quasi-particle mixing applications have yet to be produced. These applications will require (non-*RSJ*-like) high-quality, thin-film, *SIS* type junctions with low subgap conductance.

Digital Applications

Researchers with an interest in digital applications such as ultrahigh-speed analog-to-digital conversion (*ADC*) have been attracted by the fundamental properties of Josephson devices. Josephson junction are fast, with ∼1 ps switching times; have low switching power, $P \sim I^2_c R \sim 0.1\ \mu W$; and can be matched to the impedance of modern microstrip technology (69).

The most extensive effort to use Josephson devices to create a prototype superconducting computer was the much-discussed program at IBM. Although the program was not successful in achieving its ultimate goal, a great deal was learned and much progress was made (70). Lead-alloy technology that produced junctions with reproducible characteristics and that could be thermally cycled was used. The logic elements were based on latching circuitry with underdamped junctions ($\omega_p \ll \omega_c$) such that the binary state was defined by the voltage state of a Josephson junction. For example, a junction can be switched from a zero-voltage state to a nonzero voltage state along the load-line of the device. As discussed by 69, this type of approach has fast set times (∼1 ps) but slow reset times (∼10 ns). Other difficulties with this arrangement include problems in achieving uniform device clocking across an entire logic array and high latching power (∼1 μW) per gate. More recent work with single-flux-quantum (SFQ) logic (referring to logic based on the presence of single fluxiods in *SQUID*-based logic elements) has switched to Nb-based junctions (71,72,73,74) in a variety of formats.

A new logic type, which is fundamentally different from latching-type logic, has also been introduced. Called *RSFQ* (resistive/rapid single flux quantum) logic (69,75), it is a hybrid logic family, wherein junctions are configured to have both logic and (dynamic) memory functions and logic operations are performed on pulses originating from traditional SFQ devices. This approach addresses to some extent a major problem that was encountered in the IBM experimt: matching SFQ logic and memory elements. The approach also recovers much of the fundamentally fast switching times and low switching power of Josephson devices (the latter since junctions are open for only a small part of a clock period). Switching powers of $\sim 10^{-7}$ W/gate (10^{-18} J/bit) implies that packing densities of 10^7 gates/cm^2 are possible at speeds to $\sim$500 GHz with 1 μm linewidths and at greater speeds for narrower lines (4).

In present practice, much of the effort is not in computing per se but high-speed digital processing, especially *ADC* [and agile programmable voltage standards (76,77)] with *RSFQ* as a favored digital logic format (78,79). For example, 1024-bit shift registers have been operated at up to 20 GHz (80).

The current application of Josephson technology is still largely based on niobium. Niobium technology is mature and now appears to be the standard for digital Josephson applications. Niobium based junctions are physically robust and amenable to large-scale integration as a result of the important innovation of replacing the native oxide that grows on niobium, which generally forms a poor quality barrier with a relatively large dielectric constant (140 fF/μm^2) (81,82). The idea is that the niobium base electrode is capped in situ with a thin aluminum film ($\sim$1 nm to 8 nm thick), which is oxidized to completion to form a surface-layer junction and in the process prevents the growth of NbOx (9,83,84). This scheme successfully combines the relatively high critical temperature, T_c, of the (robust) Nb underlayer (9.25 K) with the unsurpassed qualities of Al_2O_3, which is an excellent barrier material with a relatively low dielectric constant (60 fF/μm^2) (84) compared with Nb oxide. A large-scale process for creating many such junctions with a simple anodization process was developed by 85,86). Likharev has reviewed the complexities of junction fabrication for digital and other applications (4).

A good example of contemporary large-scale Josephson technology is the work at HYPRES Inc., which produces large-scale integrated Nb-based Josephson tunnel junction circuitry using *RSFQ* logic. A recently manufactured large-scale integration *ADC* is shown in Fig. 9. Target applications for such systems would include high-resolution *ADCs* for radar and time-to-digital converters (*TDCs*) to measure the timing of events in high-energy and nuclear physics experiments. These systems have demonstrated flash *ADC* with 6-bit resolution, in the 1 GHz to 10 GHz operating range (87).

Another potential application for the fast switching speed of Josephson junctions is cross-bar and related switching matrices for switching between processors and memory (88,89). This is important to high-speed telecommunications and computation applications.

We finally note that other approaches based on quantum-limited-logic have been proposed and may be competitive in some areas. One of these is single-electron logic (*SEL*), which is based on charging effects in ultrasmall capacitance tunnel junctions (and not the Josephson effect). *SEL* is operationally similar to *RSFQ* logic, but the former is based on the presence or absence of single electrons rather than magnetic fluxoids (loosely speaking, bits based on single electrons with charge e as opposed to single fluxoids with flux Φ_0) (4,69).

High-Temperature Superconductor Systems

The appearance of high-temperature superconductor materials has spurred a broad-based effort to produce Josephson junctions for digital and other applications. Some of these approaches were discussed previously in connection with *SQUIDs*. Beside this work, other approaches have been taken to produce a successful junction format. Certainly all the high-speed applications that are envisioned for niobium-based Josephson technology such as flash *ADC*, wideband *ADCs*, transient-event digitizers, and crowbar switches could be envisioned for high-temperature superconductor materials as well. Barring thermodynamic considerations, operation at higher temperatures would generally be an advantage. The biggest hurdle now for high-temperature

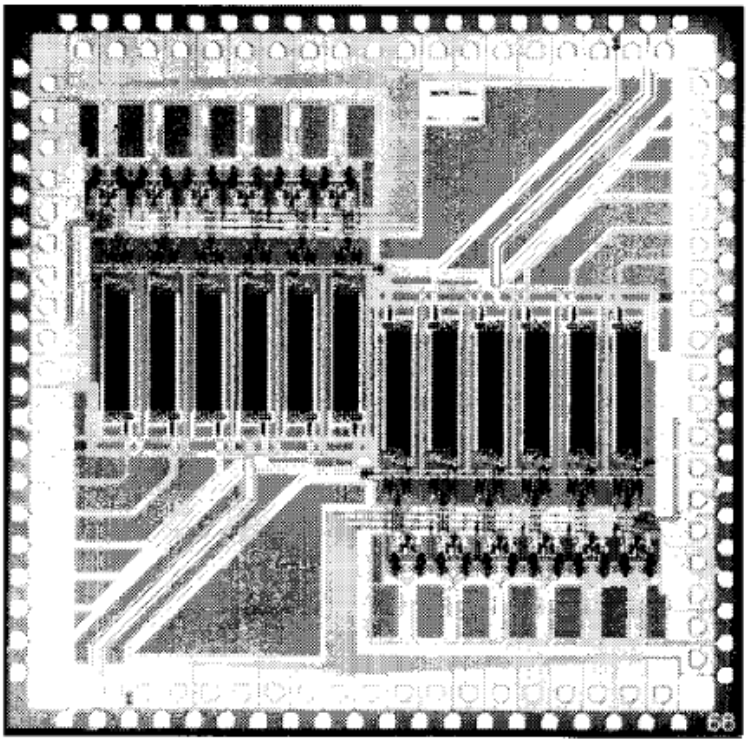

Fig. 9. Modern analog/digital converter from HYPRES, Inc. using niobium technology. The chip is a 6-bit flash *ADC* with a 32-word shift resister memory and operates at 16 GS/s.

superconductor digital applications is the uniformity of the Josephson critical current density (Josephson critical current per unit junction area) for junctions across a single chip and chip-to-chip critical current uniformity. A maximum variation of a few percentage points in critical current density is probably necessary for large-scale applications (90), and this has yet to be achieved. At present, achievable spreads in critical current density are more in the vicinity of (or perhaps somewhat less than) 10 percent. This single consideration is a dominant factor governing which basic device format will be successful for high-temperature superconducting materials, a number of which have been and are currently being explored in an attempt to find a suitable candidate to meet this criterion.

We again note that high-temperature superconductors can be viewed as quasi-two-dimensional materials—a stack of Josephson coupled two-dimensional superconducting layers. This basic physical structure, combined with a propensity for naturally occurring grain boundaries—which also act as Josephson weak links—has led to the investigation of intrinsic Josephson effects (91,92,93,94,95,96,97,98,99). Some of the devices based on naturally occurring, intergranular weak links have exhibited good critical-current and normal-state characteristics. However, the use of naturally occurring weak links to create junctions per se has typically lead to poor reproducibility. Focused ion beam (*FIB*) techniques have also been used in an attempt to artificially induce defects at given locations by inducing substrate damage (100).

A successful approach to creating SNS type junctions in preselected locations is focused electron beam (*FEB*) writing. Here, an electron beam is directed at a location on a superconducting thin film, creating a narrow, damaged line of material. The material then acts as a normal metal to create an *HTS*/N/*HTS* (*HTS*, high-temperature superconductor) device (101,102,103,104,105,106). The technique can produce *RSJ*-like

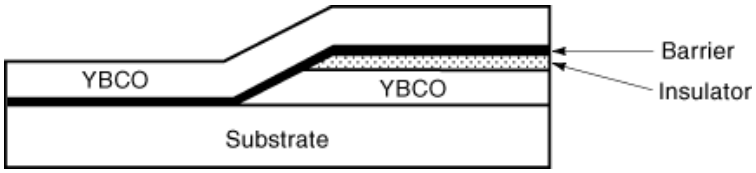

Fig. 10. Sketch of the ramp junction geometry used with high-temperature superconductor materials, shown here with YBaCuO films.

microwave behavior (107,108). An example is the work at Cambridge (104), where a computer-controlled electron beam (350 KeV at 400 pA) is swept across narrow lines of YBaCuO. This process has produced junctions with an SNS character (17) with long-term room-temperature stability. One drawback of the large-scale use of *FEB* is its slow materials processing speed, since each device must be individually electron-beam written.

High-Temperature Superconductor Ramp Junctions. The idea of creating a step in a substrate has also been extended to make SNS and *SIS* type structures where the normal and insulating materials are separately introduced films as opposed to defect-modified high-temperature superconductor material. Originally, SNS junctions used normal metals such as gold; however, such devices appear to have been dominated by interface resistance. More recently, both cobalt-doped YBaCuO and gallium-doped PrBaCaO have been used as generic barrier materials in YBCO/barrier/YBCO systems, selected because they are physically compatible with YBaCuO and their conductance properties can be tuned with doping level. Cobalt-doped YBaCuO has a relatively low resistance, as opposed to gallium-doped PrBaCuO, and thus imposes a somewhat limited device operating temperature range because the material becomes superconducting below some temperature (109), although relatively narrow critical current density spreads (∼12 percent variation) have been observed with the material (110,111). Such junctions have also been employed in *SQUIDs* (112).

Gallium-doped PrBaCuO tunnel barriers tend to produce relatively high resistance barriers and must be operated below 77 K. Nevertheless, the material can produce junctions with values of I_cR in a technologically useful range (∼1 mV) and with independently adjustable critical current density and resistance (113), which is important for engineering considerations. In one view of tunneling in PrBaCuO, supercurrent (zero-voltage) conduction occurs via direct tunneling through the barrier whereas quasi-particle (nonzero-voltage) conduction occurs via resonant tunneling channels within the barrier (114). The fundamentals of this issue were also addressed, with device applications in mind, by work with amorphous silicon barriers (115).

HTS/I/*HTS* tunnel junctions using PrBaCuO barriers in a ramp format have been produced through a variety of techniques (116,117). A sketch of the standard ramp junction format used with high-temperature superconductor materials is shown in Fig. 10. All tend to produce devices with *RSJ*-like characteristics [with I_cR ∼ 1 mV at 4.2 K, which scales with PrBaCuO doping (118)]. The combination of step-edge substrates and doped barriers has been promising overall, and these devices have been modeled by microscopic theory (17), although the full applicability of standard proximity-effect theory with regard to high-temperature superconductor materials remains an open question (119).

To date, small circuits have been put together with these junctions, which are designed with tolerance to the large spreads that exist at present in junction critical current (120,121,122,123,124). Clearly, again, the challenge is to improve on the reproducibility of critical currents in this or any other device configuration that may present itself.

Related to this work are engineered interface YBaCuO/I/YBaCuO–type junctions. Here, the barriers are produced by relatively subtle damage to the base YBaCuO film and then YBaCuO is simply deposited on top. The suggestion is that the barrier comprises a thin layer of YBaCuO with oxygen disorder or deficiency perhaps a few nanometers thick (125). Other groups have been experimenting with this and related techniques (126).

In summary, a variety of promising approaches have been explored with high-temperature superconductor materials to produce junctions for *SQUID* and digital applications. The primary goal is to produce junctions

that are parametrically reproducible, and the secondary goal is to produce a thin-film barrier compatible with the high-temperature superconductor materials with transport properties close to the metal–insulator transition. The latter would allow the junction to be self-shunting and thus allow for a broader use of the devices. This balancing act is challenging in light of the problems of material compatibility with high-temperature superconductor systems and unanswered questions regarding the physics of barriers (especially high-temperature superconductor-compatible materials) near the metal–insulator transition.

High-Temperature Superconductor Applications:Technical Considerations. A great deal of effort has gone into the application of high-temperature superconductor materials for *SQUIDs* and SFQ/*RSFQ* logic circuitry. Such circuits need nonhysteretic junctions with $I_c \sim 50$ μA to 500 μA and $R \sim 1$ Ω for $10 < T < 77$ K, which is achieved with low-temperature superconductors at 4.2 K by shunting. In the case of high-temperature superconductor materials, compatible barrier materials—such as doped PrBaCuO or YBaCuO—typically have far lower resistivities than barriers such as Al_2O_3. Therefore, as noted, these barrier materials have been examined with a view toward obtaining high-temperature superconductor–based junctions in the parametrically desirable region where shunting would be unnecessary (109,127,128).

In Likharev's description of SFQ circuits (129) it was shown that for niobium junctions with $I_cR \sim 0.2$ mV, operation can be in the 100 GHz range. For SFQ to work, one needs series or parallel loops of junctions with inductance L such that $(1/2)\Phi_0 < LI_c < (3/2)\Phi_0$. This limits the acceptable range of I_c for junctions. A lumped-parameter analysis (130) indicates that at ~10 K the minimum I_c for $I_cR \sim 0.1$ mV to 1.0 mV is ~0.2 m and for high temperatures, ~60 K to 70 K, I_c will need to be ~1.2 mA. The analysis also indicates that to avoid latching and ensure sufficiently fast signal propagation, the condition on junction resistance will be that $R_{max} \sim 4$ Ω for $\epsilon_r = 40$ with 1 μm lines and 2 Ω for $\epsilon_r = 100$, where ϵ_r is the dielectric constant of the material adjacent to the signal lines.

This analysis and the results of other work (131,132) suggest that devices using PrBaCuO-based barriers can achieve critical currents, I_c, in the range of 10^5 A/cm^2 and still be nonhysteretic. The ultimate conclusion is that that PrBaCuO barriers can give junctions parametrically compatible with SFQ applications.

Three-Terminal Devices

One overriding characteristic of a Josephson junction is that it is a two-terminal device, more like a forward-biased diode with a hysteretic current-voltage characteristic than a transistor, which has a gate or base terminal. However, there have been a number of proposed and experimentally examined three-terminal superconducting devices. These include hybrid superconductor–semiconductor devices, such as junction and field-effect transistors, and nonequilibrium superconducting devices, such as stacked-junctions and injection-controlled weak links (133). At present none of these devices has found its way into standard use, because they generally have not exhibited above unity gain, although in theory this appears to be possible (134). One inherent problem is the high carrier density of conventional superconducting materials, making it difficult to modulate device transconductance. However, high-temperature superconductor materials, which have far lower carrier densities and perhaps other parametric advantages for certain device configurations (135), provide somewhat more promise for three-terminal devices.

Early work on Josephson FETs per se has included InAlAs/InGaAs *HEMT*-type configurations, where a gate controls the magnitude of the Josephson current (136). The overall prospects for Josephson FETs (137), and experimental results with HEMPT devices (138) have also been presented. Generally it appears ultimately possible to create a device with voltage gain, driving loads of ~100 Ω. FET-type structures have also been created in YBaCuO/barrier/YBaCuO *SIS*-type systems, where a base layer is used to apply a strong electric field across the barrier region using an external gate, causing a change in surface carrier density and a corresponding modulation of the Josephson current. Examples of this work include YBaCuO/$SrTiO_3$/YBaCuO and related structures (139,140,141,142,143,144,145,146) and Au/$SrTiO_3$/YBaCuO (NIS) structures (147,148).

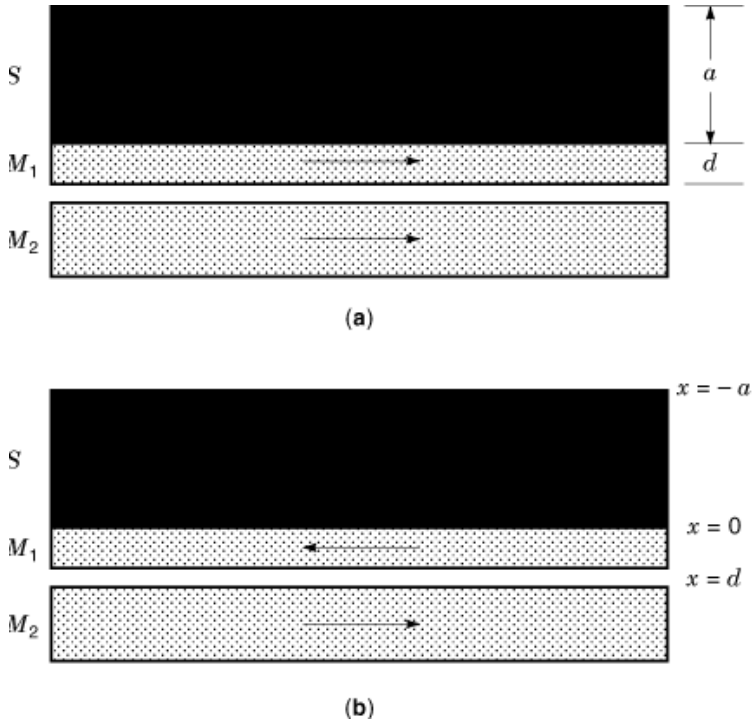

Fig. 11. The figure shows the structure of a proposed magnetic/superconductor memory element. Shown are parallel (a) and antiparallel (b) configurations of magnetization in the M layers. Figure from Sangjun et al., Ref. 170.

In general, FET structures have to date not shown anything but relatively weak effects, although work on a variety of promising systems continues (149). The work is motivated in part because the devices have the potential to serve as a Josephson-to-semiconductor logic interface. The general problem to be addressed is that Josephson logic output voltages are ∼3 mV (for low-temperature superconductors) while a CMOS device operates at ∼1 V. Some work has been specifically directed at this issue (150,151), including interface electronics combining 4 K Josephson drivers and 77 K semiconducting *HEMT* amplifiers with a predicted speed of 1 GHz to 3 GHz (152).

A variety of other schemes have also been advanced for both low- and high-temperature systems. These fall under the generic categories of electric-field controlled devices (153,154,155,156,157), quasi-particle injection devices (158,159), flux-flow transistors (160,161), and dielectric-base transistors (66,162,163,164,165).

Although these ideas continued to be pursued, an achievable device format with useful gain has yet to emerge unambiguously. Certainly, three-terminal high-temperature superconductor devices will require higher quality junctions and for FETs, dielectric gates compatible with high-temperature superconductor materials and better geometries to provide improved coupling of electric fields into junctions. Thorough discussions of three-terminal Josephseon devices are available in the literature (155,167,168,169).

Related Superconducting Devices

While not superconducting tunneling devices, several systems have recently been developed that could interface with superconducting devices and logic. One example, illustrated in Fig. 11, is a memory element based on superconductor–magnetic multilayers (170).

There has also recently been considerable interest in the physics and device implications of tunnel junctions containing magnetic elements (171,172,173,174,175), which may also be compatible with and complementary to Josephson circuitry.

Acknowledgments

I wish to thank Alan Kleinsasser for many useful comments on the text. I also wish to acknowledge insightful discussions with M. R. Beasley, D. A. Moore, J. M. Rowell, and J. Talvacchio and comments by Alan Kadin. I also gratefully acknowledge support during the preparation of this work by the Department of Energy, Division of Materials Sciences, through grant DE-FG02-88ER45373.

BIBLIOGRAPHY

1. T. Van Duzer C. W. Turner *Principles of Superconductive Devices and Circuits*, New York: Elsevier North Holland, 1981.
2. A. Barone G. Paterno *Principles and Applications of the Josephson Effect*, New York: Wiley, 1982.
3. A. Barone G. Patterson *Physics and Application of the Josephson Effect*, New York: Wiley, 1982.
4. K. K. Likharev *Dynamics of Josephson Junctions and Circuits*, New York: Gordon and Breach, 1986.
5. H. Weinstock M. Nisenoff *Superconducting Electronics*, Berlin: Springer-Verlag, 1989.
6. J. C. Gallop *SQUIDs, the Josephson Effects and Superconducting Electronics*, New York: Adam Hilger, 1990.
7. S. T. Ruggiero D. A. Rudman *Superconducting Devices*, New York: Academic Press, 1990.
8. T. P. Orlando K. A. Delin *Foundations of Applied Superconductivity*, Reading, MA: Addison-Wesley, 1991.
9. S. T. Ruggiero Artificial tunnel barriers, in S. T. Ruggiero, D. A. Rudman (eds.), *Superconducting Devices*, New York: Academic Press, 1990, pp. 373–390.
10. I. Giaever Metal-insulator-metal tunneling, in E. Burstein and S. Lundqvist (eds.), *Tunneling Phenomena in Solids*, New York: Plenum, 1969, pp. 19–30.
11. J. G. Simmons Low-voltage current-voltage relationships of tunnel junctions, *J. Appl. Phys.*, **34**: 238, 1963.
12. J. G. Simmons Image force in metal-oxide-metal tunnel junctions, in E. Burnstein and S. Lundqvist (eds.), *Tunneling Phenomena in Solids*, New York: Plenum, 1969, pp. 135–148.
13. S. M. Sze *Physics of Semiconductor Devices*, New York: Wiley, 1981.
14. B. D. Josephson Possible new effects in superconducting tunneling, *Phys. Lett.*, **1**: 251, 1962.
15. B. D. Josephson The discovery of tunneling supercurrents, *Science*, **184**: 527, 1974.
16. P. W. Anderson J. M. Rowell Probable observation of the Josephson superconducting tunneling effect, *Phys. Rev. Lett.*, **10**: 230, 1963.
17. K. A. Delin W. A. Kleinsasser Stationary properties of high-critical-temperature proximity effect Josephson junctions, *Supercond. Sci. Technol.*, **9**: 227, 1996.
18. J. Lukens Josephson arrays as high frequency sources, in S. T. Ruggiero and D. A. Rudman (eds.), *Superconducting Devices*, New York: Academic Press, 1990, pp. 135–167.
19. S. P. Benz Superconductor-normal-superconductor junctions for programmable voltage standards, *Appl. Phys. Lett.*, **67**: 2714, 1995.
20. C. A. Hamilton C. J. Burroughs S. P. Benz Josephson voltage standard—a review, *IEEE Trans. Appl. Supercon.*, **7**: 3756, 1997.
21. S. P. Benz, *et al.* Stable 1 volt programmable voltage standard, *Appl. Phys. Lett.*, **71**: 1866, 1997.
22. L. Fritsch, *et al.* Superconductor–normal metal–superconductor Josephson junctions with Ti interlayer, *Appl. Phys. Lett.*, **73**: 1583, 1998.
23. I. P. Nevirkovets Fabrication, dc characteristics of vertically stacked *SIS*-type structures for use as low-temperature detectors, *Supercond. Sci. Technol.*, **8**: 575, 1995.
24. A. V. Ustinov H. Kohlstedt C. Heiden Coherent flux-flow in vertically stacked long Josephson tunnel junctions, *IEEE Trans. Appl. Superconduct.*, **5**: 2743, 1995.

25. A. Shoji T. Kikuchi H. Yamamori Uniformity of critical currents of vertically stacked Josephson junctions, in *Extended Abstr. 5th Int. Workshop High-Temp. Supercond. Electron Devices*, Tokyo, **FED-157**: 157, 1997.
26. M. G. Blamire, *et al.* Characteristics of vertically-stacked planar tunnel junction structures, *IEEE Trans. Magn.*, **MAG-25**: 1135, 1989.
27. I. P. Nevirkovets L. P. Stryzhko A. V. Poladich Photon-assisted tunneling in stacked tunnel structures by millimeter wave irradiation, *Physica B*, **194–196**: 2395, 1994.
28. S. Lomatch E. D. Rippert J. B. Ketterson Multilayer Josephson junction flux quantum devices, *IEEE Trans. Appl. Supercond.*, **5**: 3147, 1995.
29. M. Scheuerman J. T. Chen J. J. Chang Interaction between microwaves and a single vortex in a long Josephson tunnel junction, *J. Appl. Phys.*, **54**: 3286, 1983.
30. S. Yoshikawa, *et al.* Intrinsic Josephson junctions of$Tl_2Ba_2Ca\ CuO_x$ thin films for high frequency devices, *Physica C*, **293**: 44, 1997.
31. M. Tinkham *Introduction to Superconductivity*, 2nd ed., New York: McGraw-Hill, 1996.
32. N. Miyakawa, *et al.* Strong dependence of the superconducting gap on oxygen doping from tunneling measurements on $Bi_2\ Sr_2\ Cau_2\ O_{7-\delta}$, *Phys. Rev. Lett.*, **80**: 157, 1998.
33. A. W. Kleinsasser R. A. Buhrman High-quality submicron niobium tunnel junctions with reactive-ion-beam oxidation, *Appl. Phys. Lett.*, **37**: 841, 1980.
34. D. J. van Harlingen R. H. Koch J. Clarke Dc *SQUID* near the quantum noise limit, *Physica (Utrech)*, **B108**: 1083, 1981.
35. D. J. van Harlingen R. H. Koch J. Clarke Superconducting quantum interference device with very low magnetic flux noise energy, *Appl. Phys. Lett.*, **41**: 197, 1982.
36. Y. Zhang, *et al.* Applications of high-temperature *SQUIDs*, *Appl. Supercond.*, **3**: 367, 1995.
37. F. Ludwig, *et al.* Multilayer magnetometers based on high-T_c *SQUIDs*, *Appl. Supercond.*, **3**: 383, 1995.
38. G. L. Romani The use of *SQUIDs* in the study of biomagnetic fields, in H.-D. Hahlbohm and H. Lubbig (eds.), *SQUID '85.* Berlin: de Gruyer, 1985.
39. J. Clarke *SQUIDs*: Principles, noise and applications, in S. T. Ruggiero and D. A. Rudman (eds.), *Superconducting Devices*, New York: Academic Press, 1990, pp. 51–99.
40. J. Gao, *et al.* Controlled preparation of all high-T_c SNS-type edge junctions and dc *SQUIDs*, *Physica C*, **171**: 126, 1990.
41. C. L. Jia, *et al.* Microstructure of epitaxial $YBa_2\ Cu_3\ O_7$ films on step-edge SrTiO, *Physica C*, **175**: 545, 1991.
42. R. B. Laibowitz, *et al.* All high T_c edge junctions and *SQUIDs*, *Appl. Phys. Lett.*, **56**: 686, 1990.
43. Y. A. Boikov, *et al.* Biepitaxial Josephson junctions with high critical current density based on $YBa_2/Cu_3/O_{7-\delta}$ films on silicon on sapphire, *J. Appl. Phys.*, **77**: 1654, 1995.
44. B. N. Hunt, *et al.* High-T_c edge-geometry SNS weak link on silicon-on-sapphire substrates, *Physica C*, **230**: 141, 1994.
45. M. J. Burns, *et al.* Demonstration of$YBa_2\ Cu_3\ O_{7-\delta}$ and complementary metal-oxide-semiconductor device fabrication on the same sapphire substrate, *Appl. Phys. Lett.*, **63**: 1282, 1993.
46. D. Koelle, *et al.* High performance dc *SQUID* magnetometers with single layer $YBa_2/Cu_3/O_{7-x}$ flux transformers, *Appl. Phys. Lett.*, **63**: 3630, 1993.
47. R. Cantor, *et al.* Low-noise, single-layer $YBa_2/Cu_3/O_{7-x}$ dc *SQUID* magnetometers at 77 K, *IEEE Trans. Appl. Supercond.*, **5**: 2927, 1995.
48. F. Dillnn V. N. Giyantsev M. Siegel Performance of$YBa_2/Cu_3/O_{7-\delta}$ direct current *SQUIDs* with high-resistance, *Appl. Phys. Lett.*, **69**: 1948, 1996.
49. T. Amrein, *et al.* Thin film $Bi_2Sr_2CaCu_2O_{8+x}$ Josephson junctions and direct current superconducting quantum interference devices on (001) $SrTiO_3$ bicrystals, *Appl. Phys. Lett.*, **63**: 1978, 1993.
50. T. Takami, *et al.* Dc superconducting quantum interference devices with BiSrCaCuO bicrystal grain boundary junctions at 77 K, *Jpn. J. Appl. Phys.*, **35**: L391, 1996.
51. C. Carr, *et al.* Electromagnetic nondestructive evaluation: Moving *HTS SQUIDs*, including field nulling and dual frequency measurements, *IEEE Trans. Appl. Supercond.*, **7**: 3275, 1997.
52. L. Hao J. C. Macfarlane C. M. Pegrum Excess noise in $YBa_2Cu_3O_7$ thin film grain boundary Josephson junctions and devices, *Supercond. Sci. Technol.*, **9**: 678, 1996.
53. J. Z. Sun, *et al.* Improved process for high-T_c superconducting step-edge junctions, *Appl. Phys. Lett.*, **63**: 1561, 1993.

54. A. Cochran, *et al.* Experimental results in non-destructive evaluation with *HTS SQUIDs*, in *Proc. EUCAS '95*, Institute Physics Conf., **2**: 1511, 1995.
55. L. N. Morgan, *et al.* Electromagnetic nondestructive evaluation with simple *HTS SQUIDs*: Measurements and modeling, *IEEE Trans. Appl. Supercond.*, **5**: 3127, 1995.
56. Q. Hu P. L. Richards Quasiparticle mixers and detectors, in S. T. Ruggiero and D. A. Rudman (eds.), *Superconducting Devices*, New York: Academic Press, 1990, pp. 169–196.
57. J. R. Tucker M. J. Feldman Quantum detection at millimeter wavelengths, *Rev. Mod. Phys.*, **57**: 1055, 1985.
58. P. L. Richards Q. Hu Superconducting components for infrared and millimeter-wave receivers, *Proc. IEEE*, **77**: 1233, 1989.
59. J. A. Stern, *et al.* NbN/MgO/NbN *SIS* tunnel junctions for sub mm wave mixers, *IEEE Trans. Magn.*, **25**: 1054, 1989.
60. W. R. McGrath, *et al.* Performance of NbN superconductive tunnel junctions as *SIS* mixers at 205 GHz, *IEEE Trans. Magn.*, **27**: 2650, 1991.
61. W. Zhen A. Kawakami Y. Uzawa NbN/AlN/NbN tunnel junctions with high current density up to 54 kA/cm^2, *Appl. Phys. Lett.*, **70**: 114, 1997.
62. Y. Uzawa, *et al.* Submillimeter wave responses in NbN/AlN/NbN tunnel junctions, *Appl. Phys. Lett.*, **66**: 1992, 1995.
63. Y. Uzawa W. Zhen A. Kawakami Quasi-optical submillimeter-wave mixeres with NbN/AlN/NbN tunnel junctions, *Appl. Phys. Lett.*, **69**: 2435, 1996.
64. P. Dielman, *et al.* Shot noise in NbN *SIS* junctions suitable for THz radiation detection, in Appl. Superconductivity, *Proc. of EUCAS 1997 3rd. Eur. Conf. Appl. Superconductivity*, **1**: 421, 1997.
65. J. Chen, *et al.* $YBa_2Cu_3O_{7-\delta}$ angle grain boundary junction on Si bicrystal substrate, *Jp. J. Appl. Phys.*, **30**: 1964, 1991
66. P. Seidel S. Linzen F. Schmidl High-T_c thin films and Josephson junctions on silicon and sapphire substrates, in *Extended Abstr. 5th Int. Workshop High-Temp. Supercond. Electron Devices*, Tokyo, **FED-157**: 178, 1997.
67. P. A. Rosenthal E. N. Grossman Terahertz Shapiro steps in high temperature SNS Josephson junctions, *IEEE Trans. Microw. Theory Tech.*, **42**: 547, 1994.
68. K. Nakajima *et al.* THz response of YBCO grain boundary junctions, in *Extended Abstr. 5th Int. Workshop High-Temp. Supercond. Electron Devices*, Tokyo, **FED-157**: 185, 1997.
69. K. K. Likharev V. K. Semenow A. B. Zorin New possibilities for superconductor devices, in S. T. Ruggiero and D. A. Rudman (eds.), *Superconducting Devices*, New York: Academic Press, 1990, pp. 1–49.
70. Collection of articles, *IBM J. Res. Develop.*, **24**, 1980.
71. S. Kotani *et al.* Feasibility of an ultra-high-speed Josephson multiplier, *IEEE J. Solid-State Circuits.*, **SC-22**: 98, 1987.
72. H. Hayakawa Computing, in S. T. Ruggiero, D. A. Rudman (eds.), *Superconducting Devices*, New York: Academic Press, 1990, pp. 101–134.
73. T. van Duzer G. Lee Digital signal processing, in S. T. Ruggiero and D. A. Rudman (eds.), *Superconducting Devices*, New York: Academic Press, 1990, pp. 197–225.
74. R. S. Withers Wideband analog signal processing, in S. T. Ruggiero and D. A. Rudman (eds.), *Superconducting Devices*, New York: Academic Press, 1990, pp. 227–272.
75. K. K. Likharev O. A. Mukhanov V. K. Semenov Resistive single flux quantum logic for the Josephson-junction digital technology, in H.-D. Hahlbohm and H. Lubbig (eds.) *SQUID '85*, Berlin: de Gruyer, 1985, pp. 1103–1108.
76. S. P. Benz C. J. Burroughs C. A. Hamilton Operating margins for a pulse-driven programmable voltage standard, *IEEE Trans. Appl. Supercond.*, **7**: 2653, 1997.
77. S. P. Benz C. A. Hamilton A pulse-driven programmable Josephson voltage standard, *Appl. Phys. Lett.*, **68**: 3171, 1996.
78. K. K. Likharev V. K. Semenov *RSFQ* logic/memory family: A new Josephson-junction technology for sub-teraherz-clock-frequency digital systems, *IEEE Trans. Appl. Supercond.*, **1**: 3, 1991.
79. K. K. Likharev Ultrafast superconducting electronics: *RSFQ* technology roadmap, *Proc. Low Temp. Phys. Conf. LT-21*, 1996.
80. O. A. Mukhanov *RSFQ* 1024-bit shift register for acquisition memory, *IEEE Trans. Appl. Supercond.*, **3**: 3102, 1993.
81. J. H. Magerlein Specific capacitance of Josephson tunnel junctions, *IEEE Trans. Magn.*, **17**: 286, 1981.
82. R. F. Broom *et al.* Niobium oxide-barrier tunnel junction, *IEEE Trans. Elect. Dev.*, **ED-27**: 1998, 1980.
83. E. L. Wolf, *et al.* Proximity electron tunneling spectroscopy I. Experiments on Nb, *J. Low Temp. Phys.*, **40**: 19, 1980.

84. M. Gurvitch M. A. Washington H. A. Huggins High quality refractory tunnel junctions using thin aluminum layers, *Appl. Phys. Lett.*, **42**: 472, 1983.
85. H. Kroger L. N. Smith D. W. Jillie Selective niobium anodization process for fabricating Josephson tunnel junctions, *Appl. Phys. Lett.*, **39**: 280, 1981.
86. D. Jillie *et al.* All-refractor, Josephson logic circuits, *IEEE J. Sol. State Circuits*, **SC-18**: 173, 1983.
87. P. Bradley A 6-bit Josephson flash A/D converter with GHz input bandwidth, *IEEE Trans. Appl. Supercond.*, **3**: 2550, 1993.
88. T. Sterling P. Messina P. H. Smith *Enabling Technologies for Petaflops Computing*, Cambridge, MA, MIT Press, 1996.
89. N. B. Dubash P.-F. Yuh V. V. Brozenets SFQ data communication switch, *IEEE Trans. Appl. Supercond.*, **7**: 2681, 1997.
90. D. L. Miller J. X. Przybysz J. H. Kang Margins and yields of SFQ circuits in *HTS* materials, *IEEE Trans. Appl. Supercond.*, **3**: 2728, 1993.
91. Y. Ishimaru *et al.* Observation of boundary Josephson junction with d-wave pairing characteristics, *Jpn. J. Appl. Phys.*, **34**: L1532, 1995.
92. R. Kleiner, *et al.* Intrinsic Josephson effects in high-T_c superconductors, *Phys. Rev.*, **B49**: 1327, 1994.
93. R. Kleiner, *et al.* Dynamic behavior of Josephson-coupled layered structures, *Phys. Rev.*, **B50**: 3942, 1994.
94. A. Irie G. Oya Flux flow behavior in the intrinsic Josephson junctions in $Bi_2Sr_2CaCu_2O_y$ single crystals, *Physica C*, **235**: 3277, 1994.
95. Y. I. Latyshev J. E. Nevelskaya P. Monceau Dimensional crossover for intrinsic dc Josephson effect in $Bi_2Sr_2CaCu_2O_8$ 2212 single crystal whiskers, *Phys. Rev. Lett.*, **77**: 932, 1996.
96. A. Yurgens, *et al.* Strong temperature dependence of the c-axis gap parameter of $Bi_2Sr_2CaCu_2O_{8+\delta}$ intrinsic Josephson junctions, *Phys. Rev.*, **B53**: R8887, 1996.
97. A. Irie M. Sakakibara G. Oya Growth and tunneling properties of $(Bi,Pb)_2Sr_2CaCu_2O_y$ single crystals, *IEICE Trans. Electron*, **E77-C**: 1191, 1994.
98. A. Irie G. Oya Microwave response of intrinsic Josephson junctions in BSCCO single crystals, *IEEE Trans. Appl. Supercond.*, **5**: 3267, 1995.
99. A. Irie M. Iwama G. Oya Novel microwave-induced steps of intrinsic Josephson junctions in mesa-shaped BSCCO single crystals, *Supercond. Sci. Technol.*, **9**: A14, 1996.
100. C. Neumann *et al.* Fabrication of high I_cR_n YBCO-Josephson-junctions on MgO-substrates using a focused-ion-beam system, *Physica*, **C210**: 138, 1993.
101. A. J. Pauza *et al.* High-T_c Josephson junctions by electron beam irradiation, *IEEE Trans. Appl. Supercond.*, **3**: 2405, 1993.
102. S. K. Tolpygo, *et al.* Normal-state properties and Josephson effects in *HTS* weak links produced by electron beam, *IEEE Trans. Appl. Supercond.*, **5**: 2521, 1995.
103. B. A. Davidson *et al.* Superconductor-normal-superconductor behavior of Josephson junctions scribed in $Y_1Ba_2Cu_3O_{7-\delta}$ by a high-brightness electron source, *Appl. Phys. Lett.*, **68**: 3811, 1996.
104. D. F. Moore *et al.* Asymmetric YBaCuO Interferometers and *SQUIDs* made with focused electronbeam irradiation junctions, *IEEE Trans. Appl. Supercond.*, **7**: 2494, 1997.
105. W. E. Booij *et al.* Electrodynamics of closely coupled YBCO junctions, *IEEE Trans. Appl. Supercond.*, **7**: 3025, 1997.
106. A. J. Pauza *et al.* Electron-beam damaged high-temperature superconductor Josephson junctions, *J. Appl. Phys.*, **82**: 5612, 1997.
107. S.-J. Kim *et al.* Successful fabrication of bicrystal Si substrates for $YBa_2bCu_3O_{7-y}$ Josephson junctions, *Cryogenics*, **35**: 901, 1995.
108. S.-J. Kim *et al.* Microwave induced steps of YBCO weak link damaged by focused electron beam irradiation, in *Extended Abstr. 5th Int. Workshop on High-Temp. Supercond. Electron Devices*, Tokyo, **FED-157**, 182, 1997.
109. L. Antognazza *et al.* Proximity effect in $YBa_2Cu_3O_{7-\delta}/YBa_2Cu_{1-x}Co_x)_3O_{7-\delta}/YBa_2Cu_3O_{7-\delta}$ junctions: From the clean limit to the dirty limit with pair breaking, *Phys. Rev.*, **B51**: 8560, 1995.
110. W. H. Mallison *et al.* A multilayer $YBa_2Cu_3O_x$ Josephson junction process for digital circuit applications, *Appl. Phys. Lett.*, **68**: 3808, 1996.
111. H. Sato *et al.* Improvement in parameter spreads of YBaCuO/PrBaCuO/YBaCuO trilayer junctions, *Jpn. J. Appl. Phys.*, **35**: L1411, 1996.

112. Q. X. Jia, *et al.* Directly coupled direct current superconducting quantum interference devices based on ramp-edge Ag: YBCO/PBCO/Ag: YBCO junctions, *Appl. Phys. Lett.*, **72**: 3068, 1998.
113. M. A. J. Verhoeven High-T_c superconducting ramp-type junctions., PhD thesis, University of Twente, The Netherlands, 1996.
114. M. A. J. Verhoeven, *et al.* Ramp-type junction parameter control by Ga doping of $PrBa_2Cu_3O_{7-\delta}$ barriers, *Appl. Phys. Lett.*, **69**: 848, 1996.
115. S. J. Bending M. R. Beasley Transport processes via localized states in thin a-Si tunnel barriers, *Phys. Rev. Lett.*, **55**: 324, 1985.
116. M. A. J. Verhoeven G. J. Gerritsma H. Rogalla Ramp-type junctions with very thin PBCO barriers, in *Proc. EUCAS '95 Conf.*, Edinburg, 1995, p. 1395.
117. J. B. Barner A. W. Kleinsasser High-T_c superconductor–normal–superconductor junctions with polyimide-passivated ambient-temperature edge formation, *IEEE Trans. Appl. Supercond.*, **7**: 2502, 1997.
118. H. Myoren *et al.* Terahertz response of high-T_c ramp-type junctions on MgO, in *Extended Abstr. 5th Int. Workshop High-Temp. Supercond. Electron Devices*, Tokyo, **FED-157**: 188, 1997.
119. E. Demler *et al.* Proximity effect and Josephson coupling in the SO(5) theory of high-T_c superconductivity, *Phys. Rev. Lett.*, **80**: 2917, 1998.
120. M. A. J. Verhoeven *et al.* Ramp type *HTS* Josephson junctions with PrBaCuGaO barriers, *IEEE Trans. Appl. Supercond.*, **5**: 2095, 1995.
121. A. E. Lee J. A. Luine C. L. Pettiette-Hall Co-doped-YBCO SNS junctions for superconductive integrated circuits, *IEEE Trans. Appl. Supercond.*, **5**: 2980, 1995.
122. M. G. Forrester *et al.* A single flux quantum shift register operating at 65 K, *IEEE Trans. Appl. Supercond.*, **5**: 3401, 1995.
123. V. K. Kaplunenko Voltage divider based on submicron slits in a high T_c superconducting film and two bicrystal grain boundaries, *Appl. Phys. Lett.*, **67**: 282, 1995.
124. S. J. Berkowitz Int. Workshop on Superconductivity, High-temperature superconducting circuits using SNS long junctions transistors, *High Temperature Supercond. Electron. Fund. Appl.*, Int. Superconductivity Technol. Centre, Tokyo Japan, 1996, p. 40.
125. B. H. Moeckly, *et al.* Interface-engineering high-T_c Josephson junctions, *Appl. Supercond*, **6**: 317, 1998.
126. J. Talvacchio, private communication.
127. K. Char *HTS* SNS Josephson junctions: Interfaces and mechanisms, *Physica C*, **282–287**: 419, 1997.
128. L. Antognazza K. Char T. H. Geballe High-T_c edge junctions with YPrBaCuCoO barrier layers near the metal–insulator transition, *Appl. Phys. Lett.*, **70**: 3152, 1997.
129. S. V. Polonsky *et al.* New RSGQ circuits (Josephson junction digital devices), *IEEE Trans. Appl. Supercond.*, **3**: 2566, 1993.
130. J. Yoshida *et al.* High-T_c Josephson junction technology for digital applications, in *Extended Abstr. 5th Int. Workshop High-Temp. Supercond. Electron Devices*, Tokyo, **FED-157**: 133, 1997.
131. J. Yoshida T. Nagano Tunneling and hopping conduction via localized states in thin PBCO barriers, *Phys. Rev.*, **B55**: 11860, 1997.
132. T. Nagano, *et al.* Thin film growth for fabrication of YBaCuO/PrBaCuCoO/YBaCuO ramp-edge junctions, in *Extended Abstr. 5th Int. Workshop High-Temp. Supercond. Electron Devices*, Tokyo **FED-157**: 233, 1997.
133. A. W. Kleinsasser W. J. Gallagher Three-terminal devices, in S. T. Ruggiero and D. A. Rudman (eds.), *Superconducting Devices*, New York: Academic Press, 1990, pp. 325–372.
134. K. K. Likharev *et al.* Josephson junction with lateral injection as a vortex transistor, *IEEE Trans. Magn.*, **15**: 420, 1979.
135. W. E. Booij, *et al.* Supercurrents in closely spaced high T_c Josephson junctions, in *Proc. ATS-Workshop '96*, Twente, The Netherlands, 1996, p. 6.
136. T. Akazaki *et al.* A Josephson field effect transistor using an InAs-inserted-channel $In_{0.52}Al_{0.48}$/As/$In_{0.53}$/$Ga_{0.47}$ As inverted modulation-doped structure, *Appl. Phys. Lett.*, **68**: 418, 1996.
137. A. W. Kleinsasser T. N. Jackson Prospects for proximity effect superconducting FETs, *IEEE Trans. Magn.*, **MAG-25**: 1274, 1989.
138. H. Takayanagi T. Akazaki Superconducting three-terminal devices using *HEMT* structures, in *Extended Abstr. 5th Int. Workshop High-Temp. Supercond. Electron Devices*, Tokyo, **FED-157**: 153, 1997.

139. J. Mannhart, *et al.* Electric field effect on superconducting YBaCuO films. *Z. Phys.*, **B83**: 307, 1991.
140. X. X. X. Xi, *et al.* Electric field effects in high T_c superconducting ultrathin YBaCuO films, *Appl. Phys. Lett.*, **59**: 3470, 1992.
141. K. Matsui, *et al.* Analysis on electric field effect in Al/$SrTiO_3$/$YBa_2Cu_3O_y$ structure, *Jpn. J. Appl. Phys.*, **31**: L1342, 1992.
142. K. Joosse, *et al.* Multilayers for high-T_c superconducting electric field effect devices, *J. Alloys Comp.*, **195**: 723, 1993.
143. T. Nakamura *et al.* Study on a superconducting channel transistor, *Sumitomo Elect. Tech. Rev.*, No. 38, 35, 1994.
144. R. Schneider R. Auer Temporal response of a high-T_c superconducting field effect transistor, *Appl. Phys. Lett.*, **67**: 2075, 1995.
145. T. Nakamura H. Tokuda M. Iiyama Electric field effects of SrTiO/YBaCuO multilayers grown by all-MBE, *IEEE Trans. Appl. Supercond.*, **5**: 2875, 1995.
146. T. Fujii, *et al.* Metal–insulator–superconductor field-effect-transistor using SrTiO/YBaCuO heteroepitaxial films, *Jpn. J. Appl. Phys.*, **31**: L612, 1992.
147. T. Saito, *et al.* Fabrication of a High-T_c superconducting field effect transistor by ion beam sputtering. *IEEE Trans. Appl. Supercond.*, **7**: 3528, 1997.
148. T. Goto, *et al.* Properties of high-T_c field effect devices with ion beam sputtered SrTiO Film, in *Extended Abstr. 5th Int. Workshop High-Temp. Supercond. Electron Devices*, Tokyo, **FED-157**: 159, 1997.
149. T. Nakamura H. Inada M. Iiyama Superconducting field effect transistor of YBCO/$SrTiO_3$/YBCO tri-layer structures, in *Extended Abstr. 5th Int. Workshop High-Temp. Supercond. Electron Devices*, Tokyo, **FED-157**: 123, 1997.
150. U. Ghoshal, *et al.* CMOS amplifier designs for Josephson-CMOS interface circuits, *IEEE Trans. Appl. Supercond.*, **5**: 2640, 1995.
151. D. Crupta *et al.* Optimization of hybrid JJ/CMOS memory operating temperatures, *IEEE Trans. Appl. Supercond.*, **7**: 3307, 1997.
152. K. Hikosaka, *et al.* Josephson-semiconductor high-speed interface circuit using 77 K analog *HEMT* amplifiers, in *Extended Abstr. 5th Int. Workshop High-Temp. Supercond. Electron Devices*, Tokyo, **FED-157**: 55, 1997.
153. J. Mannhart High-T_c transistors, *Supercond. Sci. Technol.*, **9**: 49, 1996.
154. J. Chen *et al.* Possible three-terminal device with YBCO angle grain boundary, *IEEE Trans. Appl. Supercond.*, **1**: 102, 1991.
155. J. Mannhart *et al.* Large electric field effects in $YBa_2Cu_3O_{7-\delta}$ films containing weak links, *Appl. Phys. Lett.*, **62**: 630, 1993.
156. Z. G. Ivanov Field effect transistor based on a bi-crystal grain boundary Josephson junction, *IEEE Trans. Appl. Supercond.*, **3**: 2925, 1993.
157. B. Mayer J. Mannhart H. Hilgenkamp Electric field controllable Josephson junctions of high quality in high-T_c superconductors, *Appl. Phys. Lett.*, **68**: 3031, 1996.
158. I. Iguchi N. Nukui K. Lee Dynamic Cooper-pair breaking by tunnel injection of quasiparticles into a high-T_c $YBa_2Cu_3O_7$ superconductor, *Phys. Rev.*, **B50**: 457, 1994.
159. E. Kume H. Hiroyuki I. Iguchi Quasi-particle injection effect of YBCO thin films using double-injector junctions having two-holes, in *Extended Abstr. 5th Int. Workshop High-Temp. Supercond. Electron Devices*, Tokyo, **FED-157**: 167, 1997.
160. D. J. Frank M. J. Brady A. Davidson A new superconducting-base transistor, *IEEE Trans. Magn.*, **MAG-21**: 721, 1985.
161. T. Yamada, *et al.* (Ba, Rb)BiO_3 base and $YBa_2Cu_3O_x$ flux flow transistors, in *Extended Abstr. 5th Int. Workshop High-Temp. Supercond. Electron Devices*, Tokyo, **FED-157**: 142, 1997.
162. H. Tamura A. Yoshida S. Hasuo Transistor action based on field-effect controlled current injection into an insulator/$SrTiO_3$ interface, *Appl. Phys. Lett.*, **59**: 298, 1991.
163. A. Yoshida, *et al.* Dielectric-base transistor using $YBa_2Cu_3O_{7-x}$/$NdGaO_3$/$SrTiO_3$ heterostructures, *J. Appl. Phys.*, **71**: 5284, 1992.
164. T. Hato *et al.* Improved emitter-base junction with In_2O_3 in dielectric-base transistor *Jpn J. Appl. Phys.*, **34**: 6379, 1995.
165. C. Yoshida, *et al.* Electric field effect in $LaTiO_3$/$SrTiO_3$ heterostructure, *Jpn. J. Appl. Phys.*, **35**: 5691, 1996.
166. T. Hato, *et al.* Dielectric-base transistor with doped channel, *Appl. Phys. Lett.*, **70**: 2900, 1997.

167. A. W. Kleinsasser W. J. Gallagher Three-terminal devices, in S. T. Ruggiero and D. A. Rudman (eds.), *Superconducting Devices*, **372**. New York: Academic Press, 1990, pp. 325–372.
168. A. W. Kleinsasser H. Weinstock R. W. Ralston (eds.) *Superconducting Devices*, Dordrecht: Kluwer Academic, 1993, p. 249.
169. J. Mannhart Changes in the superconducting properties of high-T_c cuprates produced by applied electric fields, *Mod. Phys. Lett.*, **B6**: 555, 1992.
170. O. Sangjun D. Youm M. R. Beasley A superconductive magnetoresistive memory element using controlled exchange interaction, *Appl. Phys. Lett.*, **71**: 2376, 1997.
171. J. S. Moodera J. Nowak J. M. van de Veerdonk Interference magnetism and spin wave scattering in ferromagnetic-insulator-ferromagnet tunnel junctions, *Phys. Rev. Lett.*, **80**: 2941, 1998.
172. P. K. Wong J. E. Evetts M. G. Blamire High conductance small area magnetoresistive tunnel junctions, *Appl. Phys. Lett.*, **73**: 384, 1998.
173. S. Sankar A. E. Berkowitz D. J. Smith Spin-dependent tunneling in discontinuous Co-SiO_2 magnetic tunnel junctions, *Appl. Phys. Lett.*, **73**: 535, 1998.
174. J. Z. Sun, *et al.* Temperature and bias dependence of magnetoresistance in doped manganite thin film trilayer junctions, *Appl. Phys. Lett.*, **73**: 1008, 1998.
175. K. Inomata Y. Saito Spin-dependent tunneling through layered ferromagnetic nanoparticles, *Appl. Phys. Lett.*, **73**: 1143, 1998.

S. T. RUGGIERO
University of Notre Dame